1991-12

Sea Surface Wind Stress and Drag Coefficients: The HEXOS Results

Smith, Stuart D.; Anderson, Robert J.; Oost, Wiebe A.; Kraan, C.; Maat, Nico; DeCosmo, Janice; Katsaros, Kristina B.; Davidson, Kenneth L.; Bumke, Karl; Hasse, Lutz...

Kluwer Academic Publishing

Smith, Stuart D., et al. "Sea surface wind stress and drag coefficients: The HEXOS results." Boundary-Layer Meteorology 60.1-2 (1992): 109-142.
https://hdl.handle.net/10945/40122

SEA SURFACE WIND STRESS AND DRAG COEFFICIENTS: THE HEXOS RESULTS

STUART D. SMITH, ROBERT J. ANDERSON

Department of Fisheries and Oceans, Bedford Institute of Oceanography, P.O. Box 1006, Dartmouth, Nova Scotia, Canada B2Y 4A2;

WIEBE A. OOST, C. KRAAN, NICO MAAT

Royal Netherlands Meteorological Institute, 3730 AE deBilt, the Netherlands;

JANICE DeCOSMO, KRISTINA B. KATSAROS

Dept. of Atmospheric Sciences, University of Washington, Seattle, WA 98195, U.S.A.;

KENNETH L. DAVIDSON

Department of Meteorology, Naval Postgraduate School, Monterey, CA93943-5000;

KARL BUMKE, LUTZ HASSE

Institut für Meereskunde, Universität Kiel, D2300 Kiel, Germany;

and HELEN M. CHADWICK

UK Meteorological Office, London Road, Bracknell, Berkshire RG12 2SZ, U.K.

(Received in final form 7 December, 1991)

Abstract. Turbulent fluxes have been measured in the atmospheric surface layer from a boom extending upwind from the Dutch offshore research platform *Meetpost Noordwijk* (MPN) during HEXMAX (Humidity Exchange over the Sea Main Experiment) in October–November, 1986. We started out to study eddy flux of water vapour, but discrepancies among simultaneous measurements made with three different anemometers led us to develop methods to correct eddy correlation measurements of wind stress for flow distortion by nearby objects. We then found excellent agreement among the corrected wind stress data sets from the three anemometers on the MPN boom and with eddy correlation measurements from a mast on a tripod. Inertial-dissipation techniques gave reliable estimates of wind stress from turbulence spectra, both at MPN and at a nearby ship. The data cover a range of wave ages and the results yield new insights into the variation of sea surface wind stress with sea state; two alternative formulas are given for the nondimensional surface roughness as a function of wave age.

1. Introduction

The Humidity Exchange over the Sea (HEXOS) programme (Katsaros *et al.*, 1987; Smith *et al.*, 1983) consisted of coordinated field, laboratory and theoretical studies of sea-to-air water transport. In the HEXOS main field experiment, HEXMAX, water vapour flux and spray droplets were measured together with wind stress, heat flux, sea state, boundary-layer height and other supporting parameters (Smith *et al.*, 1990). The programme was intended primarily to study humidity exchange, and results on water vapour flux and humidity measurement techniques are reported by DeCosmo *et al.* (1992) and Katsaros *et al.* (1992).

Boundary-Layer Meteorology **60**: 109–142, 1992.

2. Description of the Experiment

HEXMAX took place from October 6 to November 28 1986 at and in the neighborhood of the Dutch offshore platform Meetpost Noordwijk (MPN). Eddy flux and dissipation measurements of evaporation, heat flux and wind stress and measurements of droplets and supporting parameters at MPN were the core of the experiment. The surrounding area was studied with instruments on a ship, on a tripod-based mast, on an aircraft, and on shore.

2.1. Wind stress measurements from MPN

MPN (Figure 1a), an offshore research platform owned and operated by Rijkswaterstaat (the Dutch Department of Harbours and Public Works), stands in 18 m of water in the North Sea, 9 km from shore at 52° 16′ 26″ N, 4° 17′ 46″ E (Figure 2). The main body of MPN has dimensions ($l \times w \times h$) of 23.5 × 12 × 7 m, with the lowest deck 11.6 m above mean sea level.

Instrument Support Boom

To find the required length of a boom to place the sensors in reasonably undisturbed airflow, a wind tunnel study was conducted on a 1:25 scale model of MPN (Wills, 1984; Oost *et al.*, 1992). In this study, the velocity profile of the marine atmospheric boundary layer was simulated and all three wind components were measured at an array of points in two vertical planes, 10 and 16 m (to scale) from the west railing of the platform. Wills (1984) measured not only mean wind speeds, but also variances and covariances of wind turbulence components. The model was rotated in 15° increments to simulate winds from 180° (southerly) to 360° (northerly).

The 10 m plane (corresponding to a boom used at MPN prior to HEXMAX) was found to be too close to the structure to obtain reliable momentum flux data. A 21 m boom was constructed and fixed to a riser 3 m behind the railing of the west face of the platform, placing the sensors 18 m upwind of the railing in westerly winds. The wind tunnel results are used to correct mean wind speeds measured in the field for flow distortion by MPN. A later section will treat correction of fluxes for local flow distortion by the boom and sensors.

The boom (Figure 1b) consisted of two sections, an 8 m inner section and a 13 m outer section. The inner section was connected to the platform at a point 6 m above the mean water level. The position of the boom, detected with three electronic levels, was controlled with guy-wires connected at the joint between the two sections and also near the end of the outer section. To reduce flow distortion effects, the boom ended in two prongs on which the instruments were mounted, with a separation of 2 m. Each prong had two flanges, one facing up and one down. For servicing of the instruments, the boom was winched to an upright position. The boom proved to be exceptionally stable in high winds. Even at a

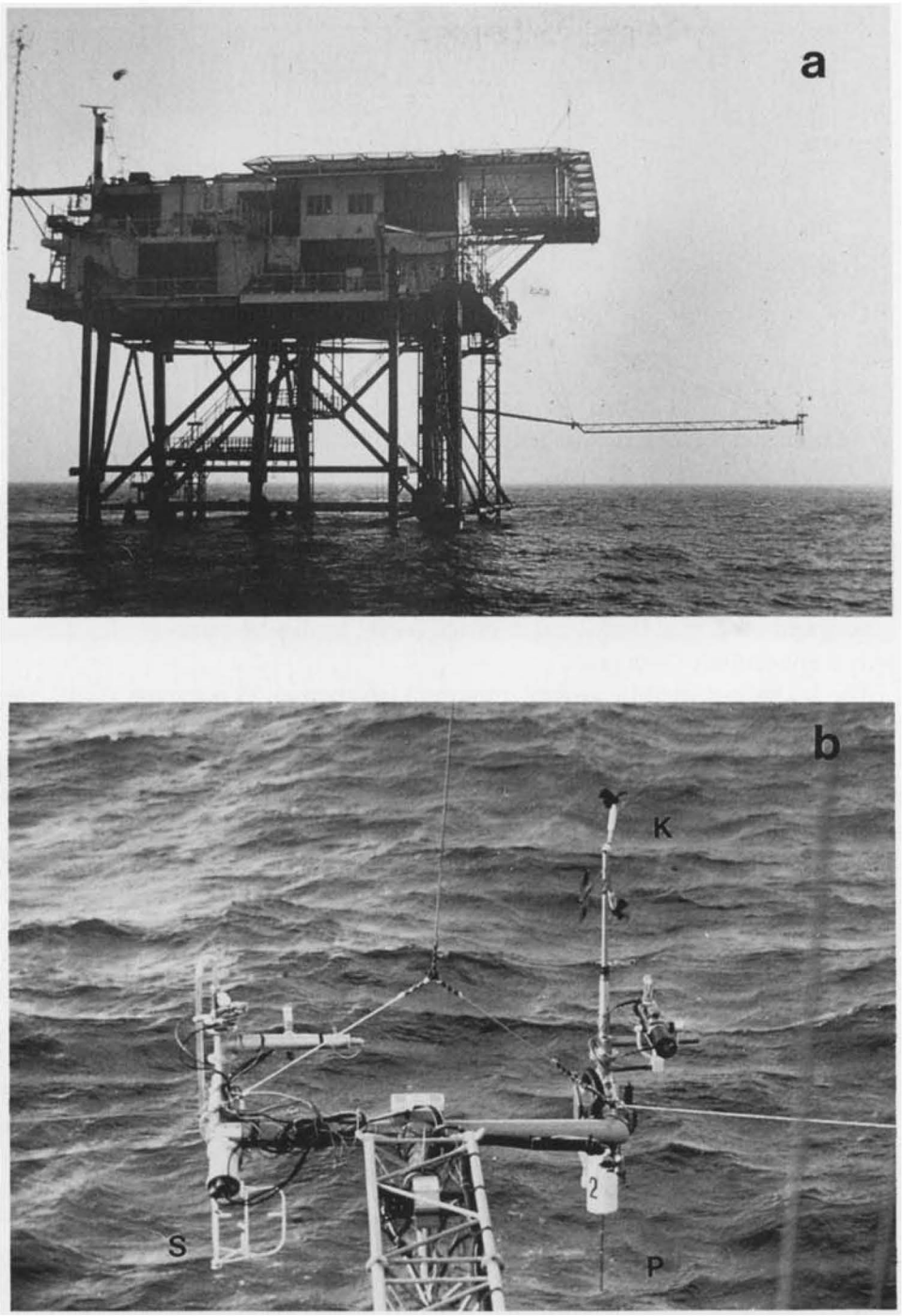

Fig. 1. (a) Meetpost Noordwijk and (b) the boom tip: (K), K-Gill anemometer; (P), pressure anemometer; (S), sonic anemometer.

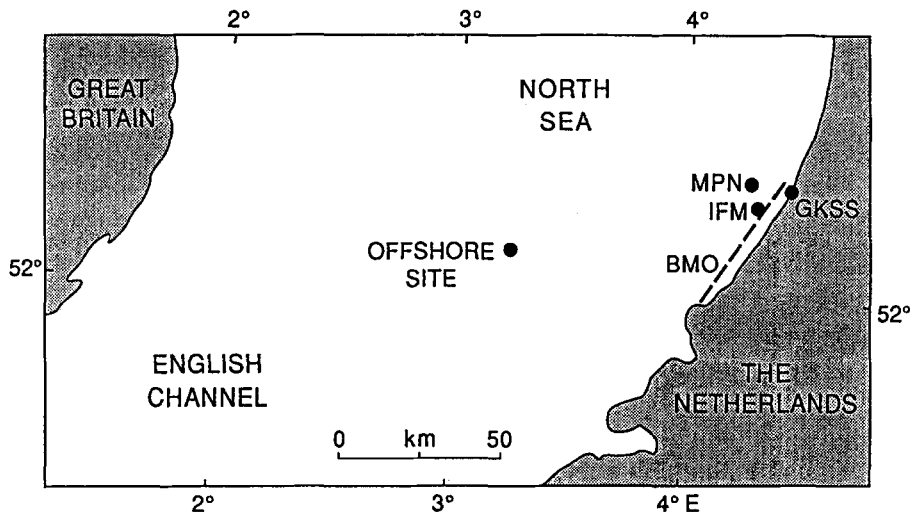

Fig. 2. The HEXMAX area: MPN, Meetpost Noordwijk; IFM, tripod site; BMO, typical flight path of C-130 aircraft; Offshore Site of RRS *Frederick Russell*; GKSS, IfM receiving station and site for radiosonde and tethersonde profiles.

wind speed of 25 m/s, the vibration of the boom, as detected with the levels, was only a few tenths of a degree.

The boom was used by groups from the University of Washington (UW), the Bedford Institute of Oceanography (BIO), the Royal Netherlands Meteorological Institute (KNMI) and the HEXIST group (Institut de Mécanique Statistique de la Turbulence, Marseilles, France; Risø National Laboratory, Denmark; Penn State University, USA; and Naval Postgraduate School, Monterey, USA) for eddy correlation and dissipation measurements of the turbulent momentum, heat and moisture fluxes and some background data (mean wind, temperature and humidity, wave height and presence of breaking waves). Three fast responding anemometers were mounted on the boom: a sonic anemometer, a "K-Gill" anemometer and a pressure anemometer.

Sonic Anemometer

A Kaijo Denki DAT-300 sonic anemometer with a TR-61 probe, owned and operated by KNMI, was the reference instrument for eddy fluxes. It has a path length of 20 cm between acoustic transducers. Each is used alternately as a transmitter and a receiver; there is one pair of transducers for each of the three direction components. This instrument has better stability than earlier models with two pairs of transducers for each component. The frequency range is 0 to 10 Hz. The probe, which allows unobstructed air flow over an azimuth range of about ±45°, was mounted on a rotor to aim it into the wind. The elevation of the sonic anemometer was 0.75 m below (or occasionally above) the boom. The data were logged by three data systems and analyzed both in the standard way, using the

factory calibration, a cosine directional response and a tilt correction (e.g., Smith, 1974) to eliminate the indicated mean vertical wind, and with a calibration/interpolation method (Oost, 1983; Kraan and Oost, 1989) developed originally for the pressure anemometer.

K-Gill Anemometer

The UW instrumentation on the boom included a K-Gill twin propeller and vane anemometer (Ataktürk and Katsaros, 1989), in addition to temperature and humidity sensors. This anemometer is well suited to the marine environment because its operation is not affected by rain or sea spray. The vertical and downwind components are derived from a pair of propellers with axes 45° above and below the horizontal. The assembly rotates on a vertical shaft and is aimed into the wind by a vane which is used also to sense the wind azimuth. A level gauge indicates any deviation of the shaft from the vertical.

Pressure Anemometer

The pressure anemometer (PA) was designed and constructed at KNMI to measure the turbulent wind vector, with emphasis on fluxes over the sea surface (Oost, 1983; Oost *et al.*, 1991). The sensor head used during HEXMAX could measure winds over a 180° range of azimuth. No rotor was required because only winds from westerly directions were used. The PA has a frequency range up to 35 Hz.

Data Logging

There were four independent time series data logging and analysis systems. The PA and sonic anemometer data were low-pass filtered at 20 Hz. The KNMI system sampled both the sonic and the PA data 70.3 times per second. The sonic data were also logged by the BIO system at 16 samples per second and analysed online by the HEXIST system. Data from the two propellers, vane and level gauge of the K-Gill anemometer and from the other UW sensors were low-pass filtered at 7 Hz, digitized at 27 Hz and logged by the UW data system.

Location of Anemometers

The flanges at the tip of the boom (Figure 1b) could be rotated on the prongs, placing the instruments either upright or upside down. The K-Gill could only be used upright and so the PA, being on the opposite flange of the north prong, was used in an inverted position. This brought its sensor head closest to the waves of the wind instruments (1.15 m below the boom). On a few occasions the PA was used in an upright position to obtain information about flow distortion; during these runs, the K-Gill could not be used. The sonic anemometer, on the south prong, was below the boom during most runs, but a few runs were made with this instrument upright.

2.2. Wind stress measurements from a fixed tripod

The group from Institut für Meereskunde, Kiel (IfM) installed a tripod on the seabed in 15 m of water at 52° 15.33′ N, 4° 20.07′ E (Figure 2), half way between MPN and the shore at Noordwijk. The tripod carried a slender mast extending 10 m above mean sea level, providing a measuring site essentially free of flow distortion (see Smith *et al.*, 1990, Figure 2). The mast supported standard sensors for mean quantities: wind speed and direction, wet- and dry-bulb air temperature, water temperature, water depth and short-wave radiation. Eddy flux instrumentation consisted of a three-dimensional orthogonal propeller system and an aspirated fast-response psychrometer. The propellers, of carbon fibre material, were mounted on a vane and oriented so that the angle of attack is approximately the same for each propeller (56°). The tripod system has been operated for a number of years in the Baltic Sea (Heßler, 1987; Behrens and Hasse, 1989).

Data Logging and Analysis

Data were telemetered by radio from the tripod to a shore station at Noordwijk. The time series of wind components occasionally had spikes caused by disturbances in the radio transmission, and disturbances (values lying outside 2.5 times the standard deviation) have been eliminated. Gaps in the time series of up to 2 samples have been filled by linear interpolation, but no more than 5% of missing data were allowed. During data analysis a wind tunnel calibration curve was applied to allow for departures of the propellers from cosine directional response. The time series were compiled in blocks of 512 s, or 2048 samples. Drag coefficients and turbulence statistics have been calculated for periods of 2 blocks, or 1024 s.

The distance constant of the propellers was determined by spectral analysis of the field data. Rolloff from the well-established $f^{-5/3}$ spectral shape of the inertial subrange at the high-frequency end of the spectra was used to derive a distance constant of 2.1 m, in excellent agreement with the manufacturer's value of 2.0 ± 0.1 m.

2.3. Shipboard wind stress measurements

Atmospheric surface-layer measurements were taken during a 6-week cruise of the RRS *Frederick Russell*. Wind stress was measured using the inertial-dissipation method by groups from the Naval Postgraduate School (NPS), Monterey, California and the Institute of Oceanographic Sciences (IOS), Wormley, U.K. using sensors located for minimal flow distortion on a 10 m mast on the foredeck (Figure 3). The IOS group measured mean wind, temperature and humidity using a propeller-vane anemometer and an aspirated psychrometer, and monitored the influence of ship motion using a two-component accelerometer. The NPS group used hot-film anemometers to sense wind turbulence. The sensors were mounted on a carriage so that they could be lowered for servicing.

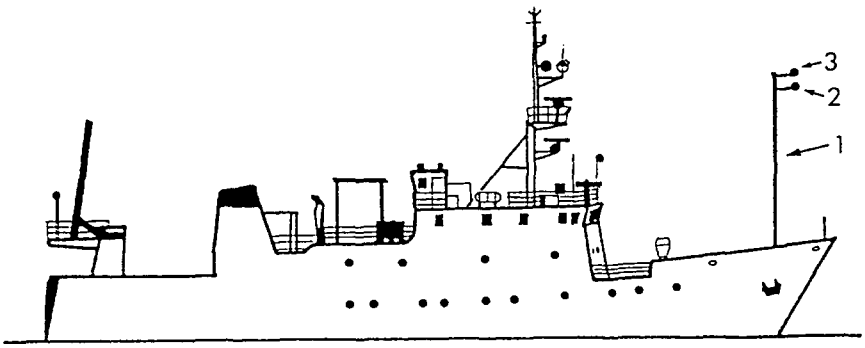

Fig. 3. Sensors on RRS *Frederick Russell*: 1. IOS 10 m mast; 2. Lower arm of carriage, holding NPS hot-film anemometers; 3. Upper arm, holding mean wind, temperature and humidity sensors.

Station Locations

To determine how representative flux measurements at MPN were of the surrounding region, the ship occupied two stations during HEXMAX. One was near MPN and the other at an Offshore Site (OS) 72 km to the west (Figure 2) where the water was slightly deeper (30 m, as compared to 18 m at MPN), and the depth was uniform over an extended upwind fetch so that coastal wave refraction was not a factor.

For minimal flow distortion during data logging periods, the ship kept the relative wind direction within ±15° of the bow by steaming into the wind at 0.5–1 m/s. After the ship had traversed about 15 km at either site she returned to station at full cruising speed. The repositioning took about 20 min after each 2–3 h period of data logging.

Data Logging

Wind spectra over a frequency band from 0.2–25 Hz were computed in real time from hot-film anemometer data. Ten-min averages of the spectra and of the wind vector, air and water temperature, humidity and pressure were logged.

Because hot-film anemometers are subject to aging, in-situ calibration was used. A calibration parameter was obtained by regression of the hot-film signal on the wind speed from the propeller-vane anemometer for each 10 min period. Variation of the calibration with time was monitored and post-processing of the hot-film anemometer data was applied if necessary. Data taken during periods of rain were not used.

Inertial-dissipation Estimates of Wind Stress

The inertial-dissipation method, extensively used by the NPS group on research ships and buoys (e.g., Guest and Davidson, 1987; Skupniewicz and Davidson, 1991; Davidson *et al.*, 1991), is suitable for estimating wind stress from shipboard measurements because it depends on the wind spectrum at frequencies higher than

those of wave-induced motion of the ship and is not affected by flow distortion provided that the sensors are suitably placed. It is less indirect than bulk estimates because it depends on turbulence statistics. The more direct eddy correlation method is generally not used from ships because it requires data over a broad band of frequencies, including those influenced by wave motion, and it requires the vertical component of wind turbulence, which is more affected by flow distortion than the downwind component. The profile method requires measurements of wind gradients at low elevations where it is nearly impossible to correct for flow distortion by the ship's hull.

The rate of dissipation of turbulent kinetic energy is

$$\epsilon = [f^{5/3} S_u(f)/(\alpha U_r^{2/3})]^{3/2} , \tag{1}$$

(e.g., Panofsky and Dutton, 1984) where U_r is the mean wind relative to the ship and S_u is its power spectrum. For frequencies f within the inertial subrange (i.e., in the band of frequencies analysed in this study), $S_u(f) \propto f^{-5/3}$. Following Fairall *et al.* (1990), a value of 0.52 is chosen for the empirical coefficient α. Assuming that measurement errors in $f^{5/3} S_u(f)$ and in U_r are about $\pm 10\%$ and that the value of α is correct, the error in ϵ is about $\pm 15\%$. Assuming that dissipation of kinetic energy is balanced by production of turbulence from the shear flow in the surface layer at the same level, the friction velocity u_* is estimated from

$$u_*^2 = [\epsilon k z/\phi_\epsilon(Z/L)]^{2/3} , \tag{2}$$

where ϕ_ϵ is a dimensionless empirical function of stratification (Z/L), the von Karman constant is $k = 0.4$ and L is the Monin–Obukhov length. The dissipation method has been "calibrated" by comparisons with simultaneous eddy flux data (e.g., Large and Pond, 1981; Fairall and Larsen, 1986; Fairall *et al.*, 1990; Edson *et al.*, 1991). Combining Equations (1) and (2),

$$u_*^2 = [f^{5/3} S_u(f)/\alpha][kz/\{U_r \phi_\epsilon(Z/L)\}]^{2/3} , \tag{3}$$

gives the wind stress $\tau = \rho u_*^2$ from measured parameters and bulk estimates of $\phi_\epsilon(Z/L)$. This is estimated with the formulation of Fairall *et al.* (1990), using bulk estimates of wind stress and sensible and latent heat flux as in (Smith, 1988) but with slightly higher drag coefficients

$$10^3 C_{10N} = 0.50 + 0.091\, U_{10N} , \tag{4}$$

obtained by averaging the results of Geernaert *et al.* (1986, Equation (22), and 1987, Equation (23)) at sites with 16 and 30 m depth, nearly the same as the depths at our two sites. For near-neutral stratification, $\phi_\epsilon(Z/L) \approx 1$. The majority of the data (77% at the OS and 70% at MPN) were taken in near-neutral conditions, $-0.05 < Z/L < 0.05$, where stratification has a small influence. In transient situations, special attention to the basic assumptions is needed.

Flow blockage by the hull and superstructure is expected to influence the mea-

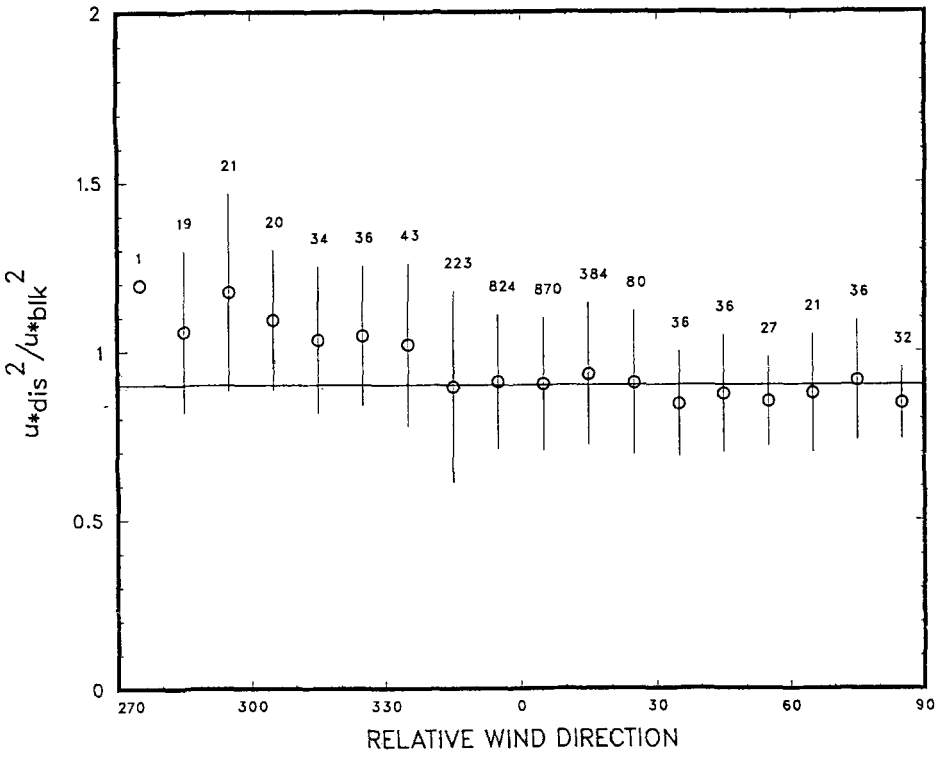

Fig. 4. Ratio of dissipation (Equation (3)) to bulk (Equation (4)) estimates of u_*^2 versus relative wind direction, in degrees clockwise from bow. Error bars show standard deviation; number of runs in each range is labelled.

sured wind least when the ship heads into the wind. In Figure 4 the ratio of the wind stress estimated by the inertial-dissipation method (Equation (3)) is compared with bulk estimates (Equation (4)) adjusted for the influence of stratification. For winds within -20 to $+30°$ clockwise of the bow, this ratio varies by less than $\pm 2\%$, while outside this range the variability is much larger. The results are used only if the mean relative wind direction is in the range -20 to $+30°$; this excludes only a few per cent of the data that may have been influenced by flow distortion.

2.4. Measurements from an instrumented aircraft

During HEXMAX, the surface-based flux measurements were supplemented by flights of the C-130 aircraft of the British Meteorological Office. This flying laboratory (Nicholls, 1978) carries instruments to measure the wind vector, air temperature and humidity, turbulent fluxes of momentum, heat and moisture, the radiative sea-surface temperature, and aerosol droplet spectra.

There were 5 flights during HEXMAX, from which turbulent flux data were

analysed for October 22 and 29 and November 11, 1986 (Table I). Fluxes were measured along a path parallel to shore passing near MPN (Leg CD), offshore from MPN (Leg AB), or parallel to shore passing near the OS (Leg GH).

2.5. Narrative of events

At the start of HEXMAX (October 6, 1986), a high pressure area over the European continent gave calm conditions ideal for the installation phase. Weak fronts passed on October 10 and 15. On October 19 an active front, associated with a depression near Iceland with a surface pressure of 970 kPa, crossed the area. A wave in this front developed into a secondary low that crossed the North Sea just north of the HEXMAX area; on October 20 the wind reached 25 m/s, the strongest wind during HEXMAX. Medium to high westerly winds prevailed during most of the remaining period. Of special interest were frontal passages with large shifts in wind direction (November 8 and 20) and a number of occurrences of surprisingly low humidity, <55%.

Favourable conditions permitted almost continuous data gathering at all stations from October 19 onward, except that on this date, the mast of the IfM tripod was broken; this is believed to be due to a collision with a boat or a drifting object. Repairs were not possible due to continuous strong winds, and the tripod was recovered only after HEXMAX was finished. Data from the tripod were obtained during the period 10–19 October at wind speeds of 4–10 m/s; there was a small overlap with the beginning of data collection at MPN.

3. Analysis and Results

3.1. Removing the influence of local flow distortion from MPN wind stress data

Flow distortion of atmospheric data is a long-standing problem (Dyer, 1973; Hunt, 1973; Izumi and Barad, 1970; Wieringa, 1980; Wucknitz, 1980; Wyngaard, 1981, 1988; Wyngaard *et al.*, 1985; Wyngaard and Zhang, 1985; Wyngaard, 1988). For eddy fluxes, the "tilt" method (e.g., Smith, 1974) is the most common correction. This assumes that any mean vertical wind is due to the sensor being tilted (imperfectly levelled) in an undistorted flow field, and the correction is made by rotating the coordinate system until the indicated mean flow is horizontal.

Initially we found good agreement in wind stress among data logging and analysis systems (Figure 5a). For 32 concurrent runs with at least 50% overlap in time, a neutral regression of independently logged and analysed BIO and HEXIST eddy stress values from the same sonic anemometer had a correlation coefficient of 0.997 and indicated general agreement to 0.05% (slope of neutral regression line = 1.000). However, the sonic anemometer indicated 20% higher stresses than the K-Gill anemometer. This is a much larger difference than calibration and analysis errors could explain, and it led us to assess in more detail both the influence of

TABLE I

Comparison of concurrent flux measurements from aircraft and MPN. Flight leg CD is parallel to the shore over MPN, AB runs offshore from MPN and GH is parallel to the shore passing over OS. MPN values of $-\overline{u_1 u_3}$ are from concurrent sonic anemometer data (BIO analysis with W81 correction).

Flight No.	Run No.	Leg	Start Time	End Time	Height m	U (30) m/s	TAIR °C	TSEA °C	QAIR g/kg	$-\overline{u_1 u_3}$ BMO $(m/s)^2$	MPN $(m/s)^2$	$\overline{tu_3}$ °C m/s	$\overline{qu_3}$ $\left(\frac{g}{kg}\right)\left(\frac{m}{s}\right)$	$10^3 C_{10N}$	Z/L
H760	3	CD	113624	114304	37.2	8.54	12.07	13.87	–	7.40E-2		7.07E-3	–	1.17	−0.18
22/10	4	CD	114644	115459	40.8	8.35	11.98	13.84	6.39	5.80E-2		8.28E-3	2.16E-2	0.93	−0.33
	9	CD	124039	124919	32.5	7.85	11.75	13.68	6.65	8.30E-2		8.48E-3	1.97E-2	1.56	−0.16
	10	AB	125559	130444	39.9	8.47	12.12	14.30	6.60	6.40E-2		9.04E-3	2.44E-2	1.02	−0.30
	11	GH	131409	132209	42.9	8.85	12.27	14.41	6.59	8.30E-2		1.28E-2	2.25E-2	1.22	−0.32
	16	GH	140609	141254	38.1	9.62	12.29	14.33	6.68	1.17E-1		1.09E-2	3.09E-2	1.54	−0.14
	Mean					8.61				0.080		0.0094	0.0238	1.24	
H762	3	CD	113758	114528	37.2	10.57	10.43	11.95	4.63	1.03E-1		6.91E-3	2.91E-2	1.17	−0.11
29/10	6	CD	121309	122208	35.8	10.80	10.51	11.88	4.49	1.05E-1	0.117	1.22E-2	3.95E-2	1.12	−0.18
	9	CD	124953	125548	34.5	10.73	10.62	11.96	4.47	1.02E-1	0.125	6.62E-2	3.74E-2	1.03	−0.10
	12	AB	132723	133633	36.3	10.49	10.68	12.64	4.49	1.11E-1		1.63E-2	4.65E-2	1.16	−0.22
	15	GH	135153	140033	38.8	10.95	10.80	13.07	4.56	1.11E-1		2.07E-2	4.23E-2	1.04	−0.30
	18	GH	142748	143528	36.2	9.95	10.85	13.11	4.71	1.09E-1		1.28E-2	4.01E-2	1.27	−0.19
	22	GH	151513	152248	35.5	11.43	11.12	13.11	4.56	1.48E-1		1.29E-2	4.18E-2	1.34	−0.11
	Mean					10.70				0.113		0.0126	0.0395	1.16	
H764	2	CD	113515	114215	37.2	13.10	12.34	10.35	6.48	9.90E-2	0.125	−1.12E-2	3.16E-3	0.78	0.19
11/11	5	CD	120910	121820	40.8	12.82	12.48	10.47	–	7.70E-2		−2.60E-3	5.83E-3	0.56	0.06
	9	CD	124355	125100	32.5	12.21	12.58	10.53	6.59	7.40E-2	0.111	−6.80E-3	2.73E-3	0.64	0.17
	12	GH	133730	134655	42.9	15.07	12.49	11.84	7.15	1.93E-1		4.85E-3	1.48E-2	1.02	−0.03
	15	GH	141255	141955	38.1	13.90	12.62	11.83	7.30	2.16E-1		−1.57E-2	−1.46E-3	0.56	0.09
	Mean					13.42				0.132		−0.0063	0.0050	0.91	

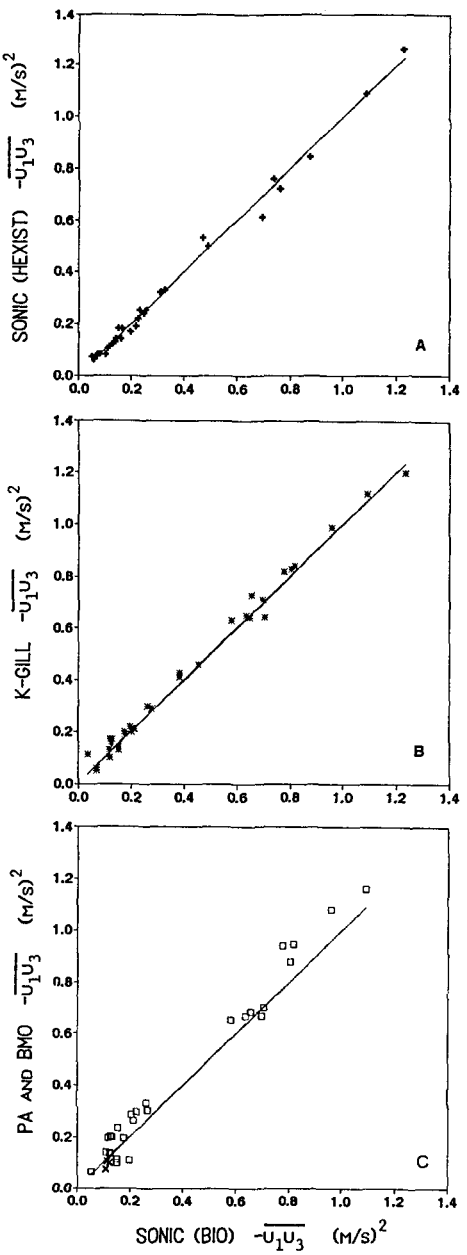

Fig. 5. (a) +, Kinematic wind stress $-\overline{u_1u_3} = u_*^2$ from KNMI Sonic anemometer with tilt corrections only by HEXIST and BIO analyses, for runs overlapping in time. (b) *, K-Gill wind stress with frequency correction, plotted against sonic wind stress (BIO analysis with W81 correction) for overlapping runs. (c) □, Corrected PA (ellipsoid method) and X, BMO from flight legs at 30 m against sonic anemometer (BIO, W81 correction) wind stresses for overlapping runs. Diagonal lines are for perfect agreement.

frequency response of the K-Gill anemometer and the influence of flow distortion by the boom and supports on all the wind data.

The Wyngaard Model

The sonic anemometer was closer to the boom than the others and was supported by a relatively bulky rotor assembly in order to aim it into the wind. On three occasions, the sonic anemometer was operated in the upright position. During these periods 5 data runs were logged by the BIO group, and these are compared with the 5 runs closest in time, in similar conditions, with the sonic anemometer in its usual inverted position. All of the data runs with the sonic anemometer inverted had negative wind tilt angles, $\vartheta_v = -1.5°$ to $-3.5°$, and higher drag coefficients than the corresponding runs with the anemometer upright. The mean drag coefficients for 5 runs were 1.39×10^{-3} with the anemometer upright and 1.89×10^{-3} with it inverted (Smith, 1991; Oost *et al.*, 1992).

Wyngaard (1981; henceforth W81) argued that the tilt correction is not sufficient to correct eddy wind stress for distortion by local objects such as probe supports. In the W81 cylinder model, the flow distortion is assumed to be due to potential flow around a horizontal cylinder which is transverse to the flow, nearby in relation to the measuring height and distant relative to its diameter. The undistorted stress, τ, is

$$\tau/\rho = u_*^2 = u_{*t}^2 + 2\overline{u_{3t}^2} \sin \theta_v \,, \tag{5}$$

where ρ is the density of air, u_3 is the vertical component of wind velocity fluctuation, $u_* = (-\overline{u_1 u_3})^{1/2}$ is the friction velocity, and the subscript t indicates results of the standard analysis with a "tilt" correction. Equation (5) also gives the correct wind stress if the distorting object is a sphere centred in a vertical plane containing the mean wind vector and the measuring point. This formula is easy to apply because the effective size and position of the distorting object need not be known except by the indicated wind tilt.

The crossbar of the boom tip is a horizontal cylinder, but is far enough from the sonic anemometer that despite its size, it accounts for only a small portion of the indicated wind tilt. Much of the wind tilt is due to the rotor, which is not spherical but is directly beneath the measuring paths. The remaining local distortion is due to the other sensors and to the sonic anemometer itself, which do not meet the criteria. Grant and Watkins (1989) found that a sonic anemometer identical to ours mounted on a pole (without the blockage of a rotor assembly) introduced a tilt of 0.9°. Nevertheless, our mean "corrected" drag coefficients were nearly identical, 1.69×10^{-3} and 1.68×10^{-3} for the "upright" and "inverted" groups, respectively (Smith, 1991; Oost *et al.*, 1992). Applying Equation (5) to all of the data with the sonic anemometer inverted (BIO analysis) reduced the wind stress by 11% on average.

Two smaller corrections have been neglected: (1) A residual tilt, depending somewhat on wind azimuth and averaging +0.7° for the 10 above-mentioned data

runs, is due to larger-scale flow distortion for which the W81 formula does not apply. The (negative) wind tilt for the runs with the sonic anemometer inverted is therefore an underestimate of the local flow distortion and we would be justified in further reducing the drag coefficients by about 3%. (2) In our test of the W81 formula, we did not adjust the drag coefficients to a common reference height. The upright position placed the anemometer at a 1.5 m higher elevation than the inverted position, where the wind speed would be higher by about 2% and the drag coefficient lower by about 4%. On this basis we have overcompensated and should not have reduced the drag coefficients as much; the neglected effect on the drag coefficient is about 2%. Fortunately these two neglected corrections are opposite in sign and are similar in magnitude.

Ellipsoid Model

The above encouraging result is not soundly based on theory and has been tested with only a small data set. To describe and correct the influence of local flow distortion on the wind stress more accurately, the W81 potential flow model was generalized to treat an ellipsoid with three unequal axes (Oost, 1991). The mean residual wind tilt for the sonic anemometer and PA data after the ellipsoid corrections is considered to be due to the influence of the platform body.

No corrections have been made for distortion of the turbulent fluxes by the platform itself. (Potential flow models cannot correct for the effect of the platform on turbulence parameters because its dimensions are not small in relation to the integral scale of the turbulence.) Britter *et al.* (1979) give reason to expect that for a circular cylinder of size comparable to the model of MPN, the correction to the fluxes at the boom tip should be negligible. The correction is very sensitive to the spectral scales of turbulence. Wills' (1984) measurements indicated that corrections of the order of 20% would be necessary, but no attempt was made in the tunnel to simulate the scales of turbulence, nor were these scales measured.

3.2. Removing the influence of tidal currents from MPN and IfM wind stress

Fairly strong tidal currents (up to about 1 m/s) in the HEXMAX area necessitated another correction to our data. At both MPN and the Kiel tripod, our wind measurements were in axes fixed to the seabed, but surface fluxes are controlled by the wind speed relative to the water surface. In most flux studies, no correction for surface current has been applied. As long as wind stresses are measured in an area where currents that are not locally driven (e.g., tidal currents) are negligible, this is no problem: in a steady state, the local wind-driven current should always be the same function of wind speed and for practical purposes it is included as part of the parameterization scheme. In this context a coordinate system moving with the tidal current is the desired frame of reference for flux results.

Surface currents are notoriously difficult to measure in the presence of surface waves and vertical shear. During HEXMAX an attempt was made to measure the

surface current using a current meter mounted beneath a float anchored near the platform. In severe wave action at the beginning of the experiment, the data tape in the current meter lost its track and this was discovered only after the instrument had been recovered at the end of the experiment. We resorted to calculation of the current profile by a relatively simple three-dimensional computer model developed for Rijkswaterstaat (Groenendijk, 1988). This model, based on Ekman dynamics, is strictly valid only for an equilibrium situation but it is tuned using data from a current meter array in the area around MPN. The original model uses empirical relations between the wind speed and the current, either near the bottom or near the water surface. We developed a variant in which vertically averaged cross-shore and longshore mass transports, from a tidal and a surge model in operational use at KNMI, were used to calculate the current as a function of depth. The other assumption used to close the equations, both in the original model and in ours, is that the cross-shore mass transport is zero. To compare our results with others in the literature, we shall take winds relative to the tidal current only, by setting the wind to zero in the model.

3.3. Wind stress analysis for the MPN boom

KNMI made two analyses of the data from the sonic anemometer and the PA, one with the tilt method, the other with a step-by-step correction for the measured tilt, the flow distortion and the surface current. The indicated wind tilt was negative on average for measurements when an anemometer was below the level of the boom and positive when it was above it. The tilt values for the PA were significantly smaller ($<1°$) than those for the sonic anemometer (2–3°). The sonic anemometer data have a larger flow distortion influence than those of the PA because the boom tip with its sensors and sensor supports, and not the platform body, was the primary cause of the distortion.

Sonic Anemometer Results

Sonic anemometer data were analysed using the KNMI and BIO systems. The data runs were inspected as strip chart records prior to analysis and periods of flawed data (e.g., "spikes" due to occasional failure to detect sonic pulses correctly) were deleted. Sonic anemometer runs reported here were not continued across sudden changes such as frontal passages.

The mean wind tilt indicated by the sonic anemometer was $-2.7°$; after correction (KNMI analysis, ellipsoid model) the residual tilt was $-0.9°$ (Oost *et al.*, 1992). The residual tilt from 5 pairs of runs (BIO analysis) with the sonic anemometer probe upright and inverted was $\sim 0.7°$, as noted above.

Pressure Anemometer Results

The tilt measured by the PA was not always consistent with its position: on a number of occasions the indicated tilt of the wind was positive with the instrument below the boom. These positive tilts ($\leq 1°$) occurred mainly with west-northwest-

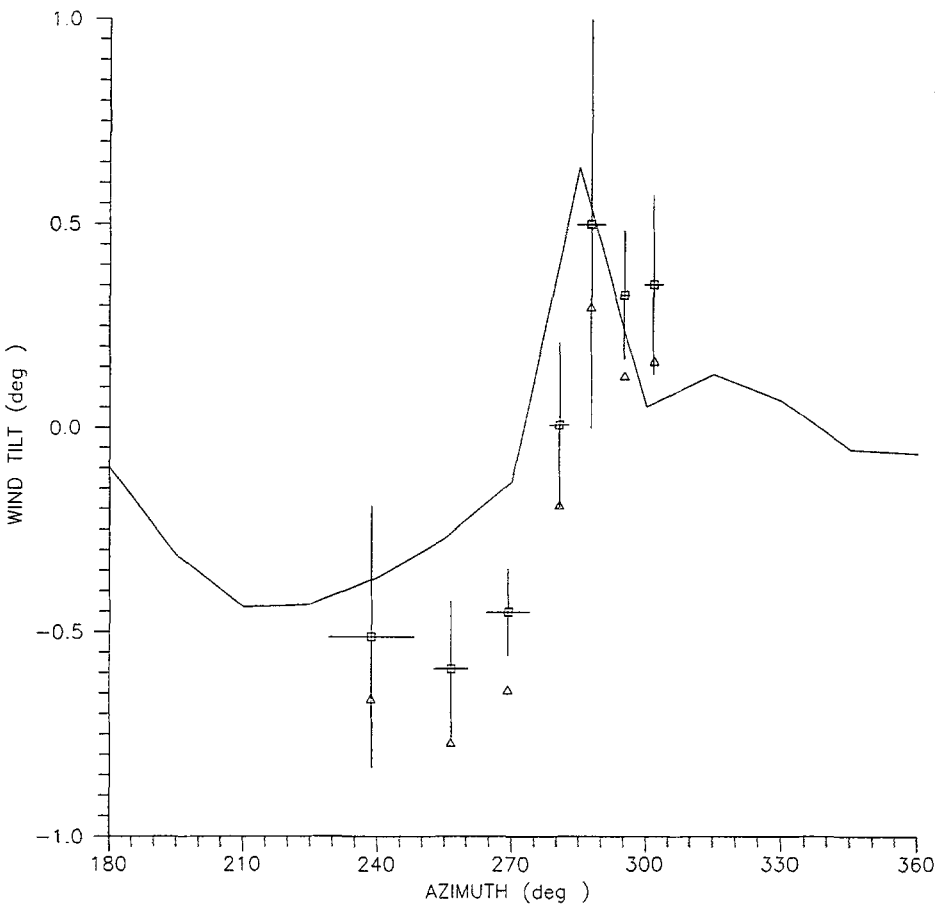

Fig. 6. The indicated wind tilt from PA data as a function of azimuth: △, raw data, averages over 5 runs grouped by azimuth; □, data corrected for local distortion with the ellipsoid model; height of crosses gives ± std error and width gives azimuth ranges of groups. Line is wind tilt due to distortion by MPN from wind tunnel study (Wills, 1984).

erly winds. This corresponds to the wind tunnel results of Wills (1984), who found positive wind tilt due to the platform body at the boom tip with a wind direction between 280 and 340° (Figure 6). These small positive tilt angles can therefore be interpreted as due to distortion by the platform body. The correspondence with the results of Wills is gratifying. Another set of positive tilt values which occurred when the wind direction was only a few degrees west of south can be explained by the influence of the other prong of the boom in the upwind direction. PA runs with "anomalous" positive wind tilt have been excluded from further analysis. Data from runs where the mean wind had an easterly component have also been deleted (the boom was on the west side of the platform). The number of runs finally retained was 36. An ellipsoid correction for flow distortion was applied, decreasing the wind stress on average by only 2.3%.

K-Gill Anemometer Results

Some 400 hours of K-Gill anemometer data were collected during HEXMAX, and 210 data runs of 45–60 min duration with relatively steady mean wind were selected for analysis. Signals from the two propellers were resolved into vertical and horizontal components using the measured tilt of the instrument shaft and an iterative scheme to correct deviations from cosine directional response of the propellers. A coordinate rotation along the mean measured wind tilt angle (the "tilt correction") was then performed to align the coordinates with the mean wind. No further correction for flow distortion by boom supports or surrounding sensors was applied, since the slender extended shaft placed the anemometer outside the calculated zone of significant distortion by these objects, according to the W81 model. At least half of the mean flow tilt measured at the K-Gill position is attributed to distortion by the platform, and no simple formula exists to describe the expected small influence of this distortion on the measured wind stress. A correction for attenuated propeller response at higher frequencies, based on the distance constant (about 3 m), was applied to the Fourier transform of the time series of winds to correct the variances and covariances (Hicks, 1972). The $\overline{u_1 u_3}$ covariance, and with it the wind stress and drag coefficient, were increased by 5–15%, depending on wind speed and on stratification.

Intercomparison of Wind Stress Results

Comparison of the K-Gill estimates of $\overline{u_1 u_3}$, or wind stress, with the sonic anemometer measurements (BIO analysis with W81 correction for flow distortion) is based on 33 data runs overlapping in time by at least 50% (Figure 5b). A neutral regression line (average of lines with each variable in turn taken as the independent variable)

$$(\overline{u_1 u_3})_{\text{K-Gill}} = 0.002\ (\text{m/s})^2 + 1.0018\ (\overline{u_1 u_3})_{\text{Sonic}}, \qquad r = 0.996\,, \tag{6}$$

shows excellent agreement.

A neutral regression for corrected PA and sonic wind stress (Figure 5c),

$$(\overline{u_1 u_3})_{\text{PA}} = 0.040 + 1.023\ (\overline{u_1 u_3})_{\text{sonic}}, \qquad r = 0.994\,, \tag{7}$$

for 22 concurrent runs again gives good agreement. Three different anemometers analysed by three data systems give equivalent wind stress results, both in concurrent runs and (as we shall see) in dependence of stress on wind speed.

Wind stress results are compared in terms of "neutral" drag coefficients adjusted to a reference height $Z = 10$ m and neutral stratification,

$$C_{ZN} = u_*^2 / U_{Zn}^2\,. \tag{8}$$

From the observed wind stress and surface roughness z_0, the reference wind speed at height Z is calculated using a neutral logarithmic wind profile,

$$U_{ZN} = (u_*/k) \ln(Z/z_0)\,. \tag{9}$$

The neutral 10 m drag coefficient increases with wind speed (relative to the tidal current), as described by neutral regression lines using the BIO analysis of the KNMI sonic anemometer data (Figure 7a),

$$10^3 C_{10N} = 0.33 + 0.112 U_{10N}, \qquad r = 0.84, n = 44\,, \tag{10a}$$

or the UW analysis of the K-Gill anemometer data (Figure 7b),

$$10^3 C_{10N} = 0.35 + 0.107\, U_{10N}, \qquad r = 0.61, \quad n = 197\,, \tag{10b}$$

or the KNMI analysis of the PA data (Figure 7c),

$$10^3 C_{10N} = 0.09 + 0.129 U_{10N}, \qquad r = 0.84, \quad n = 41\,. \tag{10c}$$

The difference among these equations is insignificant, being no larger than that due to selectively deleting 2 or 3 runs from the data sets. An average of Equations (10a–c) is our combined result for MPN,

$$10^3 C_{10N} = 0.27 + 0.116\, U_{10N}\,. \tag{11}$$

The drag coefficient at MPN increases faster with wind speed than over the open ocean (e.g., Smith, 1980, 1988), but is similar to that at other sites with similar depth (e.g., Geernaert *et al.*, 1986; $10^3 C_{10N} = 0.43 + 0.097\, U_{10N}$).

3.4. Wind stress results form the IfM tripod

Wind speeds have been adjusted relative to modelled tidal currents. Drag coefficients adjusted to neutral stratification and 10 m height (e.g., Smith, 1988, 1989) from the propeller system on the IfM tripod, using measured fluxes of sensible and latent heat to get the Monin–Obukhov stratification length, are plotted against wind speed in Figure 7d with a regression line

$$10^3\, C_{10N} = 1.11 + 0.036\, U_{10N}\,(\mathrm{m/s})\,. \tag{12}$$

This variation with wind speed is significant at the 5% level. The mean drag coefficient is $C_{10N} = 1.37 \times 10^{-3}$; the same value $(1.37 \pm 0.30) \times 10^{-3}$ is obtained from a regression of u_*^2 on U_{10N}^2, constrained to pass through the origin. Compared with the results from MPN (Equation (11)), there is a smaller dependence on wind speed. However, the agreement with the drag coefficient values from MPN is very good in the overlapping wind speed range of 6–9 m/s.

3.5. Wind stress results from RRS Frederick Russell

Comparison of Wind Stress at Offshore Site and near MPN

Similar quantities of data were gathered at the two sites, approximately 260 h near MPN and 330 h at the OS. The ship was at the OS when the highest winds occurred. Stable stratification was found 22% of the time at MPN but only 9% at the OS, while unstable air-sea temperature differences of −4 to −6 °C occurred 10% of the time at the OS but never at MPN.

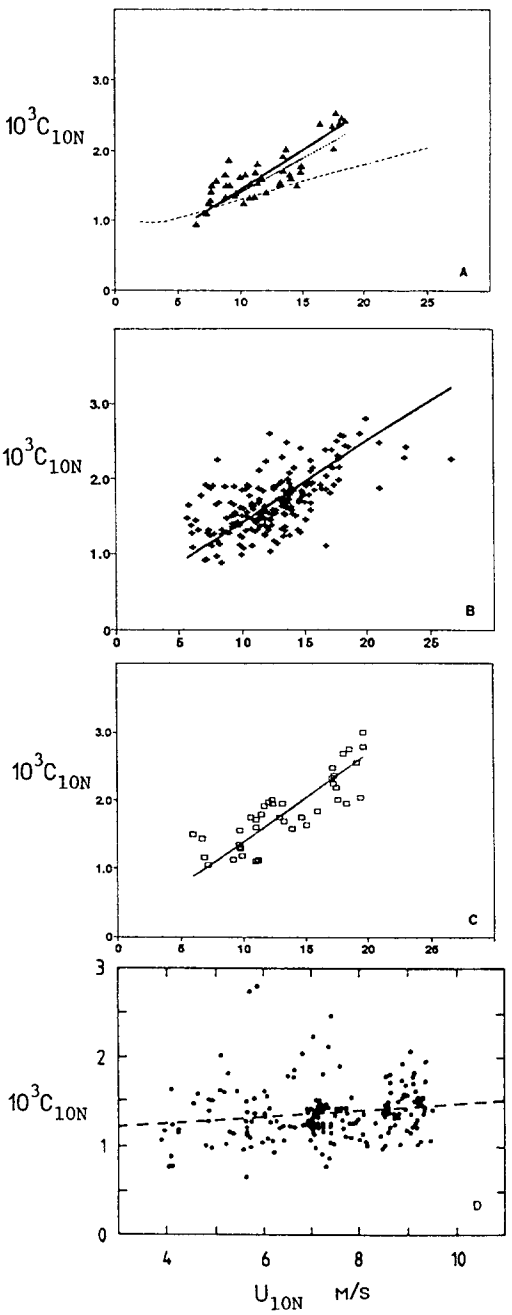

Fig. 7. C_{10N} versus U_{10N}, adjusted for tidal current. (a) BIO analysis of sonic anemometer data with W81 correction. Solid line is neutral regression, Equation (10a). Dotted line is from Geernaert *et al.*, 1986, at a site with similar depth. Dashed line is from Smith (1988) for open ocean. (b) K-Gill anemometer data, with neutral regression (Equation (10b)). (c) PA data with ellipsoid correction, with neutral regression line (Equation (10c)). All of the above at the MPN boom. (d) C_{10N} versus U_{10N} at IfM Kiel tripod, with neutral regression (Equation (12)).

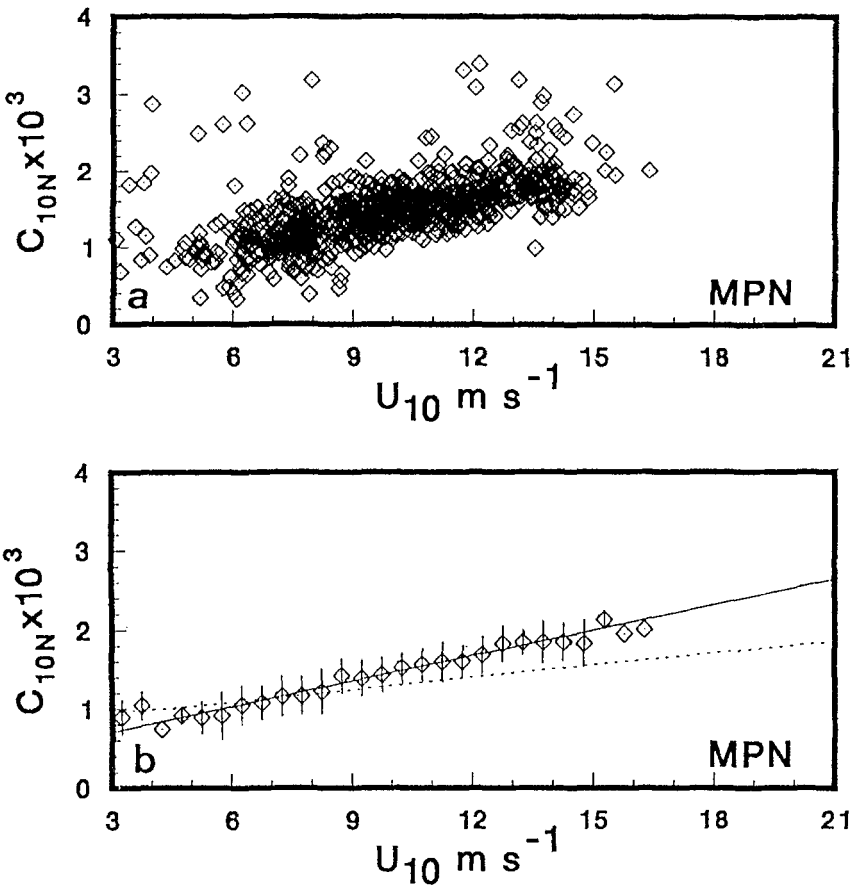

Fig. 8. C_{10N} versus U_{10N} from RRS *Frederick Russell* at MPN site, by inertial-dissipation method: (a) all points passing initial screening. (b) Means and standard deviations over 0.5 m/s intervals, with regression line (Equation (13)) and dotted line from Smith (1988).

Figures 8a and 9a show the drag coefficients as a function of neutral wind speed for the two sites. In Figures 8b and 9b, outlying points beyond 2 standard deviations from a linear least-square fit have been deleted and means and standard deviations of the remaining points are plotted in 0.5 m/s bands. Higher winds at OS, associated with the passage of storm fronts, are excluded from the linear regressions of the band averages on U_{10N}:

$$\text{MPN:} \quad 10^3 C_{10N} = 0.382\{\pm 0.034\} + 0.108\{\pm 0.003\} U_{10N}, \qquad r = 0.75\,, \tag{13}$$

$$\text{OS:} \quad 10^3 C_{10N} = 0.495\{\pm 0.035\} + 0.089\{\pm 0.003\} U_{10N}, \qquad r = 0.67\,, \tag{14}$$

where the standard errors of the coefficients are in parentheses. The results near

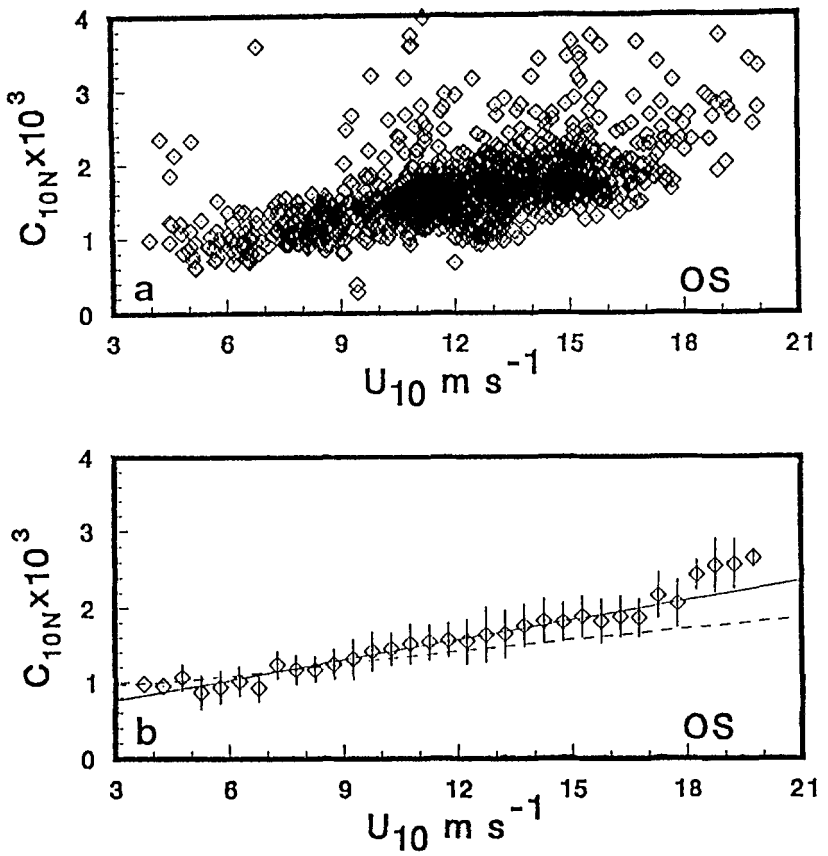

Fig. 9. C_{10N} versus U_{10N} at OS (Offshore Site). (a) All points passing initial screening. (b) Means and standard deviations over 0.5 m/s intervals, with regression line (Equation (14)) and dotted line from Smith (1988).

MPN (Equation (13)) agree well with those at MPN (Equation (11)), while at the OS, Equation (14) is almost identical with an average of the results of Geernaert *et al.* (1986 and 1987) (Equation (4)). Based on the error estimates there is a small but significant difference between the two stations. The significance of this difference was tested by calculating "cross-residuals", i.e., on comparing the values of C_{10N} near MPN with estimates from Equation (14), the null hypothesis that there is no relation between the cross-residuals and U_{10N} was rejected at the 1% level. At low wind speeds (<10 m/s), the wind stress is similar at both stations, but at higher wind speeds the shallower MPN site, where the waves cannot travel as fast as the wind, has higher wind drag. Consistency of the drag coefficients by different methods and from separate platforms at and near MPN adds to our confidence in both data sets, and we conclude that these and the IfM tripod data are characteristic of this part of the North Sea.

TABLE II

Averaged values for all legs on each flight day. Δ is per cent difference of neutral drag coefficients from MPN value (Equation (11)) for some mean wind speed.

Day 1986	U_{30} m/s	$T_s - T_a$ °C	U_{10} m/s	$10^3\ C_{10N}$ MPN	BMO	Δ %
Oct. 22	8.61	2.0	8.10	1.28	1.24	−3
Oct. 29	10.70	1.8	9.95	1.49	1.16	−22
Nov. 11	13.42	−1.5	11.94	1.73	0.91	−47

3.6. Flux results from BMO aircraft

The first flight (October 22, 1986) took place in unstable westerly flow behind a rapidly moving cold front. There were 4–5 oktas of small cumulus cloud with a base at 600 m, and widespread light showers. The second flight, on October 29, took place in a stronger westerly flow; conditions were less unstable, with 1–2 oktas of cloud and no precipitation. Sensible heat and water vapour fluxes were nearly constant during both flights at heights of 30–300 m (Chadwick, 1988), indicating a nearly constant flux from the surface to the clouds.

Profiles of wind stress on both days showed a substantial reduction with height, which may account for the stresses at 30 m being about 10–25% lower at 30 m than at the 5–7 m level of the sonic anemometer on the MPN boom (Figure 5c). There may also be differences due to the aircraft data being averaged along the flight track while the sonic anemometer data are averaged over time at a fixed point. The mean neutral 10 m drag coefficients from data at the 30 m level for each of the 3 flight days (Table II) are compared with MPN drag coefficients (Equation (11)) for 10 m wind speeds estimated from the observed 30 m wind speeds and temperature differences using Table 13 of Smith (1981b). The drag coefficient differences range from −2 to −47% with the largest difference on the day with stable stratification, suggesting that the stress decreased between the boom height and 30 m.

4. Influence of Sea State on Wind Stress

It has long been recognized that the drag coefficient of the sea surface does not depend on wind speed alone. In open-sea conditions (e.g., Smith, 1980; Large and Pond, 1981) the drag coefficient is 10–15% lower than in coastal or shallower situations (e.g., Garratt, 1977; Wu, 1980; Geernaert *et al.*, 1986, 1987), and this difference is believed to be due to a difference in typical sea states. A direct relation between wind stress and sea state is of considerable interest from a remote sensing viewpoint: the sea state in turn determines the radar reflectivity and microwave brightness temperature of the surface, which can be monitored globally by satellites.

The goal of directly relating variations of the sea surface drag coefficient to wave age (e.g., Kitaigorodskii, 1970) has remained an elusive one. Smith (1980)

attempted this but discovered that at a site exposed to the open North Atlantic, the "sea" peak in the one-dimensional wave spectrum was more often than not buried in the swell spectrum. A well-defined phase velocity c_p of "dominant" waves at the peak of the spectrum, as seen in sheltered situations (e.g., Hasselmann *et al.*, 1973), usually did not exist at this exposed site. The rms wave height, also often dominated by swell, correlated less well with the drag coefficient than did the wind speed, and relating the drag coefficient to both wind speed and wave height did not significantly improve the fit to wind speed alone.

Measurements of correlation of air pressure and wave slope (e.g., Snyder *et al.*, 1981) show that wind momentum is absorbed by young, growing waves. Nordeng (1991) estimates the influence on the drag coefficient of wave growth and of taking the wind velocity relative to the wave velocity, integrated over the wave spectrum. After a frontal passage, the waves are sometimes found to be rougher (Large and Pond, 1981; Geernaert *et al.*, 1986; Boyle *et al.*, 1987; DeCosmo, 1991). Conversely, Toba *et al.* (1989) compared ocean waves with very young (undeveloped) waves in laboratory flumes to find that the flume waves were less rough, leading these authors to propose that wave roughness increases with age.

HEXMAX offered an opportunity to study young, actively growing ocean waves. The 18 m depth at MPN limits the maximum phase velocity of surface waves to $(gh)^{1/2} = 13$ m/s. At wind speeds above 13 m/s, the waves can never match the wind speed as do mature waves in deep water. At wind speeds above 13 m/s, all of the waves can act as roughness elements and the wind drag is expected to be greater than it would be over mature waves in deep water.

4.1. Wave age parameters

The state of development of the waves is expressed by the wave age, c_p/u_* or c_p/U_{10}, where c_p is the phase speed of the dominant waves at the peak of the locally wind-driven wave spectrum. From a theoretical point of view, it is appropriate to scale with u_* (*e.g.*, Janssen *et al.*, 1987; Janssen, 1989; Perrie and Toulany, 1990), while from a practical viewpoint U_{10} is more often available. The ratio of the two parameters is $u_*/U_{10} = C_{10}^{1/2}$, and we wish to show that the drag coefficient may depend on wave age. Having noted that the two forms of the wave age are interrelated, we proceed to use mainly c_p/u_*.

A very young sea can have $c_p/u_* \simeq 5$. Fully-developed waves travel faster than the wind due to spectral transfer of energy to lower frequency, longer waves, and a fully developed sea has $c_p/U_{10} \simeq 1.2 (c_p/u_* \simeq 27\text{–}36)$, although there is no energy input from the wind for $c_p/U_{10} \geq 1.0 (c_p/u_* \geq 22\text{–}32)$.

The dimensionless peak wave frequency is $\omega_p u_*/g$ (or $\omega_p U_{10}/g$). For deep-water gravity waves, the phase speed is inversely related to frequency, $c = g/\omega$ and the wave age is simply the reciprocal of the dimensionless peak frequency. The JONSWAP experiment (Hasselmann *et al.*, 1973) has shown that there are clearly defined relations among frequency (hence wave age), fetch and wave energy, at

least for the simple case of fetch-limited growth from a shoreline in a sheltered area.

Determining the Wave Age from the Wave Spectrum

The one-dimensional wave energy spectrum $E(f)$ has been calculated from data from a wave rider buoy located about 150 m from MPN during HEXMAX. If the spectrum is found to have a single peak at f_p, we test it using a criterion

$$f_p^5 E(f_p) > 2 \times 10^{-4}, \tag{15}$$

based on the well-known Pierson-Moskovitz spectrum (see Hasselmann *et al.*, 1973); with this criterion, we were reasonably sure that the spectral peak represented an actively generated wind sea and not swell. A few of the single-peaked spectra failed to meet this criterion, in which case the wave age represented old wind sea, i.e., swell.

Some 40% of the HEXMAX wave spectra did not decrease monotonically beyond the first peak. In these cases, we first applied the above wind-sea criterion to the lowest peak frequency, and took it to determine the wave age if the criterion was satisfied. Otherwise we took the second peak at the higher frequency. These double or multiple peaks may be caused by remotely generated swell entering the area, or by a shift in the wind. The wave rider buoy measured only wave height and not direction, and so we may not have resolved crossed wave trains.

The phase speed c_p at frequency f_p is calculated using the gravity wave dispersion relation for water of finite depth d (18 m),

$$\omega^2 = gk \tanh(kd), \qquad \omega = 2\pi f, \qquad c = \omega/k\,. \tag{16}$$

For $f_p > 0.19$ Hz, the influence of depth was negligible; but in a few cases the longest waves, with $f_p = 0.11$ Hz, travelled 19% slower than in deep water.

4.2. Drag coefficient as a function of wave age

We follow the general approach of Stewart (1974) to establish the dependence of sea surface roughness (and hence the drag coefficient) on both wind speed and wave age. For mature waves the dimensionless roughness length

$$z_{0*} \equiv g z_0 / u_*^2, \tag{17}$$

is a constant, α (Charnock, 1955). For the open ocean Smith (1980, 1988) found $\alpha = 0.011$ and for compilations of results from coastal sites with presumably less mature waves, $\alpha = 0.017$ (Garratt, 1977) or 0.018 (Wu, 1980).

Maat *et al.* (1991) discussed various relationships between roughness length and wave age that have been proposed. From an earlier KNMI analysis (not corrected for flow distortion), excluding multiple-peaked wave spectra, they found for 33

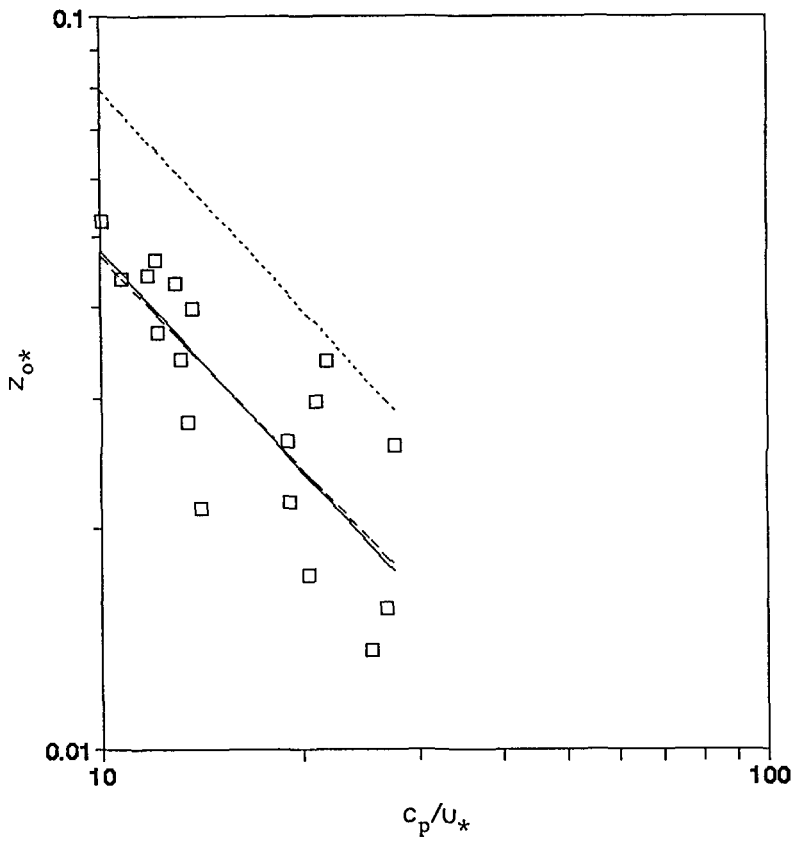

Fig. 10. Dependence of dimensionless roughness z_{0*} on wave age c_p/u_*: □, average concurrent sonic anemometer and PA data runs with single-peaked wave spectra. Dashed line is regression, solid line is Equation (18) and dotted line is from Maat *et al.* (1991, Equation (11)), $z_{0*} = 0.8(c_p/u_*)^{-1}$.

sonic anemometer runs, $z_{0*} = 0.8(c_p/u_*)^{-1}$ (dotted line in Figure 10). DeCosmo (1991, Figure 5.3) obtained a nearly identical result from the UW K-Gill anemometer data. We averaged the wind stress and wind speed from the sonic anemometer (BIO analysis with W81 correction for flow distortion) and the PA (with ellipsoid correction) for 18 concurrent runs with single-peaked wave spectra to find $z_{0*} = 0.43(c_p/u_*)^{-0.96}$, $r = 0.79$ (dashed line in Figure 10). The exponent does not differ significantly from -1. A close approximation to the regression line (solid line in Figure 10),

$$z_{0*} = 0.48(c_p/u_*)^{-1}\,, \tag{18}$$

can be taken as the HEXMAX result. In dimensional form, the influence of u_* on z_0 is seen to be proportionally 3 times stronger than that of c_p,

$$z_0 = 0.48u_*^3/gc_p\,. \tag{18a}$$

Even in the HEXMAX data set with a particularly wide range of wave ages, the

range of u_* is proportionally larger than that of c_p. This explains why in the past it has been difficult to detect the influence of c_p.

On the Hazards of Self-correlation in Scaling with u_*

We did not directly measure z_0; the roughness is derived from measured values of U and $u_* = (-\overline{u_1 u_3})^{1/2}$ using a logarithmic profile law (Equation (9)), adjusted for the influence of stratification. The exponential dependence of z_0 on u_* explains why without a modest flow distortion correction to the sonic anemometer data, a constant 67% higher than in Equation (18) was obtained by Maat *et al.* (1991). The dimensionless wave age is also calculated using the measured value of u_*. In Equation (18) and elsewhere in the literature, a power law has been fitted to a regression line to nondimensional variables, in the general form

$$\ln \bar{\mathcal{Y}} = a \ln \bar{\mathcal{X}} + b\,, \tag{19}$$

where, in near-neutral stratification, the nondimensional surface roughness is

$$\bar{\mathcal{Y}} = z_{0*} = g z_0 / u_*^2 \approx (gZ/u_*^2) e^{-kU/u_*}\,, \tag{20}$$

(noting from Equation (9) that $z_0 \approx Ze^{-kU/u_*}$) and the nondimensional wave age is

$$\bar{\mathcal{X}} = c_p/u_*\,. \tag{21}$$

The hazard of scaling both sides with u_* is that self-correlation introduced by the variability of u_* may lead to a spurious result.

In dimensional form, Equation (19) is

$$\ln[(gZ/u_*^2)e^{-\kappa U/u_*}] + a \ln u_* = a \ln c_p + b \tag{22}$$

$$\ln[(gZ/u_*^2)e^{-\kappa U/u_*} u_*^a] = a \ln c_p + b\,. \tag{22a}$$

Let $\mathcal{Y} = (gZ/u_*^2)e^{-\kappa U/u_*} \times u_*^a$, and $\mathcal{X} = c_p$. We can estimate the spuriousness introduced by the variability of u_* (Perrie and Toulany, 1990, Equation (4.8)), taking the nondimensional variables to be

$$\bar{\mathcal{Y}} = \mathcal{Y}/u_*^a \equiv \mathcal{Y}/\vartheta; \qquad \bar{\mathcal{X}} = c_p/u_* \equiv \mathcal{X}/\mathcal{U}\,, \tag{23}$$

where $\vartheta = u_*^a$ and $\mathcal{U} = u_*$. (The script variables are introduced for compatibility with Perrie and Toulany.) Negligible spurious correlation would be introduced by nondimensional scaling, $r(\ln \bar{\mathcal{Y}}, \ln \bar{\mathcal{X}}) \approx r(\ln \mathcal{Y}, \ln \mathcal{X})$, if

$$\mathrm{var}(\ln \vartheta) \ll \mathrm{var}(\ln \mathcal{Y}) \quad \text{and} \quad \mathrm{var}(\ln \mathcal{U}) \ll \mathrm{var}(\ln \mathcal{X})\,. \tag{24}$$

For the 18 runs of averaged sonic and PA data, the above are $0.146 \ll 0.486$ and $0.146 \not\ll 0.0057$. The second condition is not met: the variability of $\ln u_*$ is not smaller than that of $\ln c_p$, variation of $\ln(c_p/u_*)$ is due more to u_* than to c_p, and self-correlation has influenced the fit to obtain Equation (18). This does not disprove Equation (18) (and other results in the literature of the same general

form), but on the other hand, Equation (18) is not directly established by the HEXMAX data. As far as we know, other similar data sets would lead to the same impasse if tested for spuriousness.

Dependence of Roughness on Wave Steepness

Maat *et al.* (1991) investigated this problem by an alternate approach: they separated the variables so that there were only wave parameters on one side and wind parameters on the other. First an empirical power law

$$u_* = g^2 H_s^2/(B^2 c_p^3), \qquad r = 0.91\,, \tag{25}$$

was found, with $B = 1.04$ by fitting a regression line to a log–log plot. (This is equivalent to Toba *et al.*, 1990, Equation (16)). A substitute for wave age in terms of wave parameters only, i.e.,

$$c_p/u_* = [gH_s/Bc_p^2]^{-2}\,, \tag{25a}$$

is a function of wave steepness, $(gH_s/c_p^2) = 2\pi H_s/\lambda$, and a regression line was fitted on a log–log plot of z_{0*} (without adjustment for flow distortion) versus wave steepness,

$$z_{0*} = 0.66(gH_s/c_p^2)^{1.91} \approx 0.71(c_p/u_*)^{-0.96}, \qquad r = 0.67\,. \tag{26}$$

The two-stage process gave essentially the same result and helps to support Equation (18).

An Approach that Avoids Self-Correlation

To find out if C_{10N} depends on sea state in addition to wind speed, Smith (1991) took an alternative approach. For a small subset of the data with concurrent video and eddy flux analysis available, wave direction was estimated from video tapes of the waves (E. Monahan, pers. comm.) For these runs, the "anomaly" in the drag coefficient was calculated as the difference ΔC_{10N} between the BIO analysis of the neutral drag coefficient from the sonic anemometer data (after corrections) and values of Smith (1988) for open-ocean conditions, with $z_{0*} = 0.011$ in Equation (17). The anomaly increased rapidly for younger wave ages (Smith, 1991, Figure 2). A neutral regression,

$$10^3 \Delta C_{10N} = 1.85 - 2.24 c_p/(U_{10N} \cos\theta), \qquad r = 0.77\,, \tag{27}$$

was fitted for 10 runs with single wave trains; θ is the difference between wind and wave directions. If cases with multiple wave trains are included, the data set is twice as large but more scattered and the results are inconclusive.

Equation (27) gives zero anomaly at a wave age of 0.83, approximately the upper end of the range (0.4–0.9) of wave ages in the data subset, while the drag coefficient for young waves is nearly twice as large as for mature waves. This is qualitatively similar to our earlier result (Equation (18)), and demonstrates that

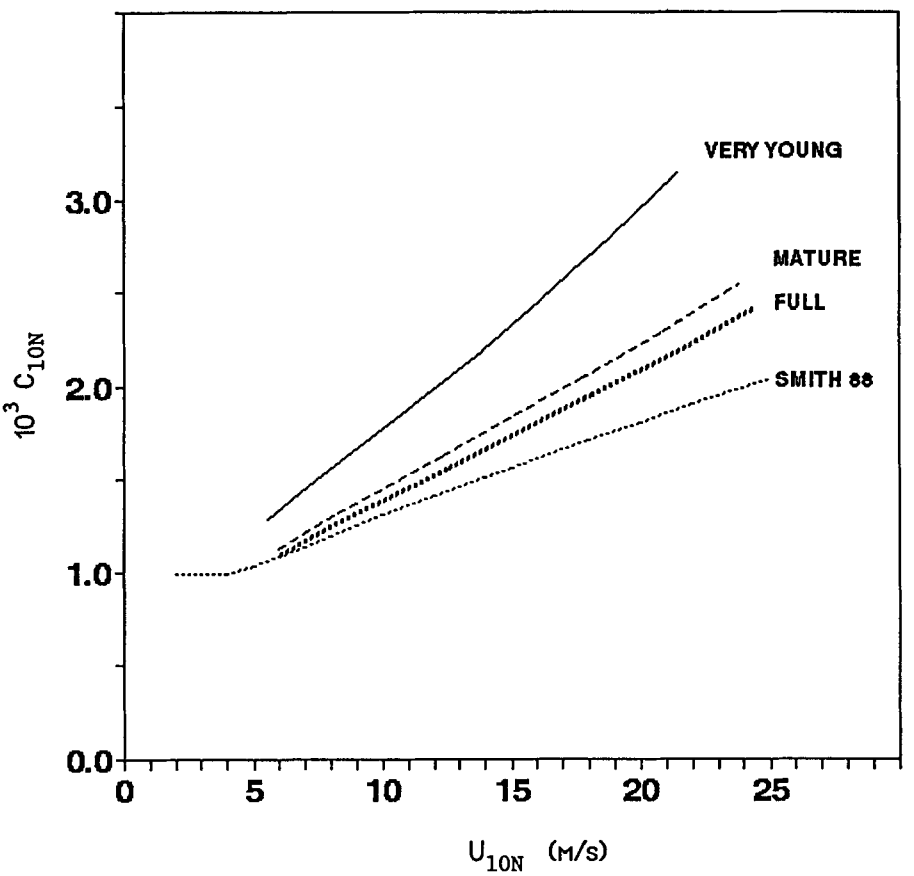

Fig. 11. Neutral drag coefficient as a function of wind speed from Equations (8), (9), (17) and (18): Solid line, very young waves, $c_p/U_{10} = 0.5$; dashed line, mature, $c_p/U_{10} = 1.0$; heavy dotted line, fully-developed, $c_p/U_{10} = 1.2$. Dotted line from Smith (1988) is lower than present result for mature waves.

even after the dependence of C_{10N} (or z_0) on wind speed is removed, there remains a significant dependence on wave age.

Perrie and Toulany (1990) found that modelling the growth of wind waves with fetch from CASP (Canadian Atlantic Storms Project) scaled with Equation (27) "results in better correlation coefficients than scaling with drag coefficients from Smith, 1988, which in turn does better than a constant C_{10}".

Discussion

Equations (8), (9) and (18) allow C_{10N}, which is a unique function of z_0, to be estimated from U_{10N} and c_p. Equation (18) is possibly influenced by spurious self-correlation through scaling with u_*, but it is supported indirectly by two other analyses of the data. The drag coefficient is larger over younger seas, but the influence of wind speed is dominant. A solution of these equations is a family of curves for C_{10N} versus U_{10N} (Figure 11) that show a stronger dependence on

wind speed for youger waves, reproducing the generally higher variation of drag coefficients with wind speed observed at sites with limited fetch or limited water depth, e.g., Greenaert *et al.* (1986, 1987), as compared to Smith (1980) or Large and Pond (1981). The variation of C_{10N} with wave age agrees qualitatively agreement with the model 3 of Janssen (1988) and Nordeng (1991).

Equation (18) gives higher values of the drag coefficient for mature waves than Smith (1980, 1988). One possible explanation is that the wind data from the offshore tower used by Smith (1980) contained tilt angles of 2–9° which were assumed to be mainly due to tilt of the tower caused by wind loading and stretch of its mooring cables. If part of the wind tilt was due to flow distortion by the instrument supports (which did not look any "cleaner" than those at MPN), then in addition to the usual tilt correction, the W81 correction would be applicable to part of the indicated wind tilt, and the drag coefficients would be higher by a few per cent. Another way to bring the results together would be to use a larger negative exponent in Equation (18), giving a smaller value of z_0 for mature waves.

After allowing for dependence on wind speed, sea state and stratification, more scatter remains in the drag coefficient than can be explained by measurement errors. Most other marine wind stress data sets have similar scatter, and this does not seem to have decreased much with modern advances in sensor technology and data handling. Some may be due to mesoscale processes on scales comparable to the length of our data runs, or to passage of large-scale low pressure systems (Geernaert *et al.*, 1986; Boyle *et al.*, 1987; DeCosmo, 1991). We noticed that when surface wave spectra had multiple peaks, the roughness lengths were considerably more scattered (points not shown in Figure 10). Smith (1991) also noted that the dependence of C_{10N} on wave age was more consistent for cases with single wave trains. Directional wave spectra will be needed to investigate the influence of complex sea states.

Effective Roughness of the Waves

Donelan (1990, Figure 12) argues that as waves become more mature, an increasing part of the wave spectrum represents waves travelling close to the wind speed and contributing little to the effective roughness. He regresses the ratio of aerodynamic roughness to rms wave height (z_0/H_{rms}) on reciprocal wave age $(c_p/U_{10})^{-1}$. He obtained quite different results from his measurements over Lake Ontario, $z_0/H_{rms} = 5.53 \times 10^{-4}\ (U_{10}/c_p)^{2.66}$, and in a wind-wave flume, $z_0/H_{rms} = 9.76 \times 10^{-6}\ (U_{10}/c_p)^{3.48}$. Flume waves have about the same ratio of roughness to height as much older waves in the field, but are much smoother than would be expected from an extrapolation of field results. Possibly the flume waves are so closely spaced that they shelter each other and contribute less efficiently to the aerodynamic roughness. All of the waves are much smoother than fixed roughness elements with z_0/H_{rms} typically ≈ 0.03.

A line fitted to the combined HEXMAX sonic and PA data (Figure 12),

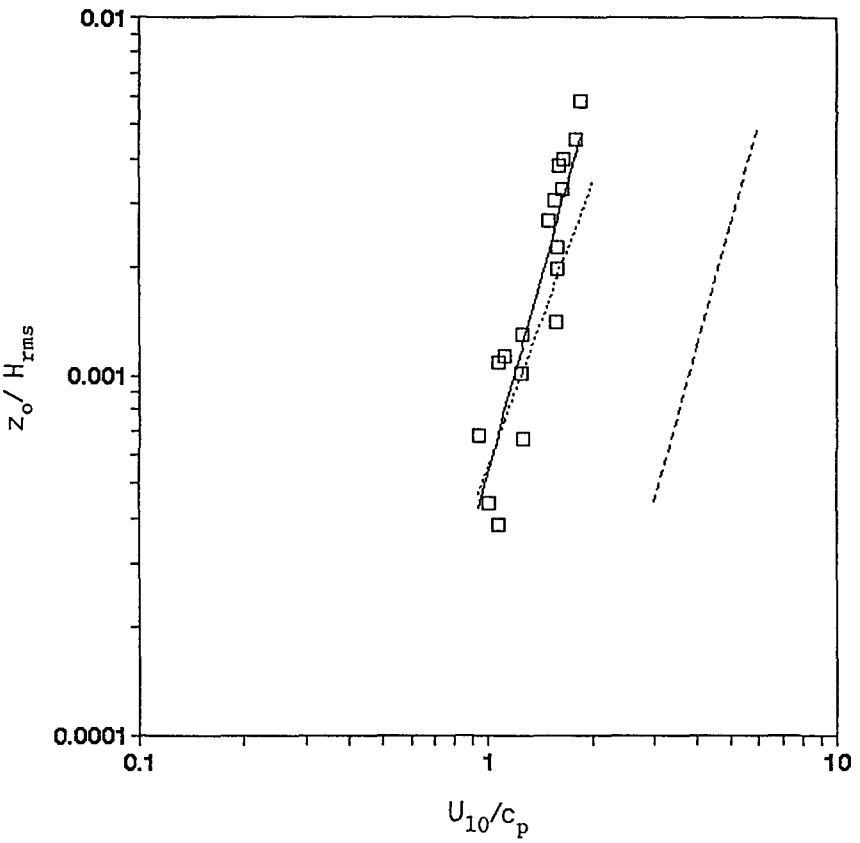

Fig. 12. Roughness length normalized with rms wave height, plotted against reciprocal wave age U_{10}/c_p: □, average of concurrent sonic anemometer and PA data runs with single-peaked wave spectra. Solid regression line is Equation (28). Dotted line is from Donelan (1990) for Lake Ontario site and dashed line is from Donelan's laboratory data.

$$z_0/H_{\rm rms} = 5.32 \times 10^{-4}(U_{10}/c_p)^{3.53}, \qquad r = 0.90, \quad n = 18\,, \tag{28}$$

confirms Donelan's field results, although the exponent most closely matches his flume results. Although Donelan's formulation has not been widely tested at this time, it uses dimensionless ratios formed from four independent parameters and so does not suffer from the same weakness as Equation (18). For satellite monitoring, this is a very useful way to relate waves, winds and surface stress.

We still have the problem that in the open ocean $H_{\rm rms}$ is dominated by swell and is not an appropriate parameter. In future experiments directional wave spectra will be measured and, on separating sea from swell, the rms height of sea only ($H_{\rm sea}$) will be used to obtain a relation analogous to Equation (28) that does not depend on the swell climate of the site.

5. Summary

Initially a sonic anemometer indicated some 20% higher wind stress than a K-Gill anemometer. The sonic anemometer data were corrected for local flow distortion. A potential flow formula based on the approach of Wyngaard (1981) brought drag coefficients from a group of runs with the probe upright into agreement with corresponding runs with the probe mounted downward. This reduced the wind stresses by 11% on average. The K-Gill anemometer was farther from the boom on a slender support where local flow distortion was negligible, but a correction for its reduced propeller response to higher-frequency fluctuations increased wind stress values by 8% on average. After these corrections, a regression analysis for 33 sonic and K-Gill anemometer runs with at least 50% overlap in time gave overall agreement within 0.2% in wind stress. Wind stress measured with a pressure anemometer also agreed with values from the sonic and K-Gill anemometers. The variation of the neutral drag coefficient with wind speed at MPN (Figure 7) is given by Equation (11).

Eddy flux data from a slender tower at a shallower (15 m) site 5 km from shore help to confirm the validity of the MPN data, but do not include higher wind speeds at which younger waves are found to have higher drag coefficients. Inertial dissipation measurements from a ship near MPN also agreed, whereas at an offshore site in slightly deeper water, the drag coefficients increased slightly less with wind speed than at MPN. Airborne flux measurements at 32 to 43 m height on a limited number of occasions gave slightly lower wind stress than concurrent measurements at MPN.

The dimensionless roughness of the sea surface is found to vary inversely with the age c_p/u_* of the dominant waves (Equation (18)). This explains why higher drag coefficients have been observed in experiments at coastal or shallow sites, where waves tend to be younger than at deeper sites with unlimited fetch. Scattered results were obtained for cases with multiple wave trains or with two or more peaks in the wave spectrum, suggesting that for mixed sea and swell, the wind stress may depend on the sea state in a more complex way. The derivation of Equation (18) is flawed by spurious self-correlation through scaling with u_*, but is indirectly supported by finding a significant dependence of z_{0*} or C_{10N} on wave age in two other ways. The Donelan (1990) scaling of z_0/H_{rms} as a function of wave age c_p/U_{10} (Equation (28)) avoids the problem of self-scaling by estimating roughness of the sea surface from wave age using parameters that can be measured either *in situ* or by remote sensing. There remains the problem that H_{rms} is often dominated by swell at open-ocean sites.

Acknowledgements

We thank J. Schaap, C. van Oort and E. Worrell of KNMI, S. S. Ataktürk and R. J. Lind of UW, D. L. Hendsbee of BIO, P. J. Boyle, S. A. Fellbaum, C. E.

Skupniewicz and D. E. Spiel of NPS, and H. Fechner, P. R. Timm and K. Uhlig of IfM. Participation of UW and NPS were funded by ONR, and of IfM by Deutsche Forschungs-gemeinschaft, SFB 133, "Warmwassersphare des Nordatlantiks". P. K. Taylor was chief scientist on board RRS *Frederick Russell*. This is Contribution 31 of the HEXOS Programme.

References

Ataktürk, S. S. and Katsaros, K. B.: 1989, 'A Twin Propeller-Vane Anemometer for Measurements of Atmospheric Turbulence', *J. Atmos. Oceanic Tech.* **6**, 509–515.

Behrens, K. and Hasse, L.: 1989, 'Mesoskalige Variabilität über See', *Annalen der Meteorologie* **26**, 209–210.

Boyle, P. J., Davidson, K. L., and Spiel, D. E.: 1987,'Characteristics of Over-Water Surface Stress During STREX', *Dyn. Atmos. Oceans* **10**, 343–358.

Britter, R. E., Hunt, J. C. R., and Mumford, J. C.: 1979, 'The Distortion of Turbulence by a Circular Cylinder', *J. Fluid Mech.* **92**, 269–301.

*Chadwick, H. M.: 1988, 'Fluxes and Transfer Coefficients Obtained by an Instrumented Aircraft During HEXMAX', in W. A. Oost, S. D. Smith, and K. B. Katsaros (eds.), *Proc. NATO Adv. Workshop HEXMAX Analysis and Interpretation*, Dept. of Atmospheric Sciences, University of Washington, Seattle, 243 pp.

Charnock, H.: 1955, 'Wind Stress on a Water Surface', *Quart. J. Roy. Meteorol. Soc.* **81**, 639–640.

Davidson, K. L., Boyle, P. J., Gautier, C., Hanson, H., and Khalsa, S.: 1991, 'Medium to Large-Scale Variability During FASINEX', *J. Geophys. Res.* **96**, 8531–8551.

DeCosmo, J.: 1991, 'Air-Sea Exchange of Momentum, Heat and Water Vapor over Whitecap Sea States', Ph.D. Dissertation, University of Washington, Seattle, 212 pp.

DeCosmo, J., Katsaros, K. B., Smith, S. D., Anderson, R. J., Oost, W. A., Kraan, C., Hasse, L., and Grant, A. L. M.: 1992, 'Fluxes of Water Vapor and Heat at the Sea Surface During HEXMAX', (in preparation).

Donelan, M. A.: 1990, 'Air-Sea Interaction', pp. 239–292 in B. LeMéhauté and D. M. Hanes (eds.), *The Sea*, Vol. 9A, Interscience – J. Wiley & Sons, New York.

Dyer, A. J.: 1973, 'Flow Distortion by Supporting Structures', *Boundary-Layer Meteorol.* **20**, 243–251.

Edson, J. B., Fairall, C. W., Larsen, S. E., and Mestayer, P. G.: 1991, 'An Experimental and Theoretical Investigation of the Inertial-Dissipation Method for Computing Air-Sea Fluxes', *J. Geophys. Res.* **96**, 10689–10711.

Fairall, C. W., Edson, J. B., Larsen, S. E., and Mestayer, P. G.: 1990, 'Inertial Dissipation Air-Sea Flux Measurements: Prototype System Using Real-Time Spectral Computations', *J. Atmos. Oceanic Tech.* **7**, 425–453.

Fairall, C. W. and Larsen, S. E.: 1986, 'Inertial-Dissipation Methods and Turbulent Fluxes at the Air-Ocean Interface', *Boundary-Layer Meteorol.* **34**, 287–301.

Garratt, J. R.: 1977, 'Review of Drag Coefficients over Oceans and Continents', *Mon. Weather Rev.* **105**, 915–929.

Geernaert, G. L., Karsaros, K. B., and Richter, K.: 1986, 'Variation of the Drag Coefficient and its Dependence on Sea State', *J. Geophys. Res.* **91**, 7667–7679.

Geernaert, G. L., Larsen, S. E., and Hansen, F.: 1987, 'Measurements of the Wind Stress, Heat Flux and Turbulence Intensity During Storm Conditions over the North Sea', *J. Geophys. Res.* **92**, 13127–13139.

Grant, A. L. M. and Watkins, R. D.: 1989, 'Errors in Turbulence Measurements with a Sonic Anemometer', *Boundary-Layer Meteorol.* **46**, 181–194.

Groenendijk, F. C.: 1988, 'Verticale structuur van de wind- en dichtheids-gedreven reststroom in de Nederlandse kustwateren', (Vertical Structure of the Wind- and Density-Driven Residual Current in Dutch Coastal Waters), Tech. Rep., Utrecht University, 101 pp. (in Dutch).

Guest, P. S. and Davidson, K. L.: 1987, 'The Effect of Observed Ice Conditions on the Drag Coefficient in the Summer East Greenland Sea Marinal Ice Zone', *J. Geophys. Res.* **92**, 6943–6954.

Hasselmann, K., Barnett, T. P., Buows, E., Carlson, H., Cartwright, D. E., Enke, K., Ewing, J. A., Gienapp, H., Hasselmann, D. E., Kneseman, P., Meerburg, A., Müller, P., Olbers, D. J., Richter, R., Sell, W., and Walden, H.: 1973, 'Measurements of Wind-Wave Growth and Swell Decay During the Joint North Sea Wave Project', *Ergänzungsheft zur Deutschen Hydrographischen Zeitschrift, Riehe A* (8°), Nr. 12, 95 pp.

Heßler, G.: 1987, 'Variability of Turbulent Momentum Fluxes over a Tideland – A Case Study', *Meroerologische Rundschau* **40**, 108–118.

Hicks, B. B.: 1972, 'Propellor Anemometers as Sensors of Atmospheric Turbulence', *Boundary-Layer Meteorol.* **3**, 214–228.

Hunt, J. C. R.: 1973, 'A Theory of Turbulent Flow Around Two-Dimensional Bluff Bodies', *J. Fluid Mech.* **61**, 625–706.

Izumi, Y. and Barad, M. L.: 1970, 'Wind Speeds as Measured by Cup and Sonic Anemometers and Influenced by Tower Structure', *J. Appl. Meteorol.* **9**, 851–856.

Janssen, P. A. E. M.: 1989, 'Wave-Induced Stress and Drag of Air Flow over Sea Waves', *J. Phys. Oceanogr.* **19**, 745–754.

Janssen, P. A. E. M., Komen, G. J., and de Voogt, W. J. P.: 1987, 'Friction Velocity Scaling in Wind Wave Generation', *Boundary-Layer Meteorol.* **38**, 29–35.

Katsaros, K. B., Smith, S. D., and Oost, W. A.: 1987, 'HEXOS – Humidity Exchange over the Sea, a Program for Research on Water-Vapor and Droplet Fluxes from Sea to Air at Moderate to High Wind Speeds', *Bull. Amer. Meteorol. Soc.* **68**, 466–476.

Katsaros, K. B., DeCosmo, J., Anderson, R. J., Smith, S. D., Kraan, C., Oost, W. A., Hasse, L., Mestayer, P. G., and Smith, M. H.: 1992, 'Measurement of Temperature and Humidity in the Marine Environment', in preparation.

Kitaigorodskii, S. A.: 1970, 'The Physics of Air-Sea Interaction', Hydrometeorological Press, Leningrad, 284 pp.; English translation, 1973, 237 pp., available as TT 72-50062 from U.S. National Technical Information Service, Springfield, VA 22151, U.S.A.

Kondo, G. and Naito, N.: 1972, 'Disturbed Wind Fields Around the Obstacle in Sheared Flow near the Ground Surface', *J. Met. Soc. Japan* **50**, 346–354.

Kraan, C. and Oost, W. A.: 1989, 'A New Way of Anemometer Calibration and its Application to a Sonic Anemometer', *J. Atmos. Oceanic. Tech.* **6**, 516–524.

Large, W. G. and Pond, S.: 1981, 'Open Ocean Momentum Flux Measurements in Moderate to Strong Winds', *J. Phys. Oceanogr.* **11**, 324–336.

Maat, N., Kraan, C., and Oost, W. A.: 1991, 'The Roughness of Wind Waves', *Boundary-Layer Meteorol.* **54**, 89–103.

Nicholls, S.: 1978, 'Measurements of Turbulence by an Instrumented Aircraft in a Convective Boundary Layer over the Sea', *Quart. J. Roy. Meteorol. Soc.* **104**, 653–676.

Nordeng, T. E.: 1991, 'On the wave age dependent drag coefficient and roughness length at sea', *J. Geophys. Res.* **96**, 7167–7174.

Oost, W. A.: 1983, 'The Pressure Anemometer – an Instrument for Adverse Circumstances', *J. Clim. Appl. Meteor.* **22**, 2075–2084.

Oost, W. A.: 1991, 'Flow Distortion by an Ellipsoid and its Application to the Analysis of Atmospheric Measurements', *J. Atmos. Oceanic Technol.* **8**, 331–340.

Oost, W. A., Worrell, E. H. W., Schaap, J. W., van Oort, C., and Kraan, C.: 1991, 'An Improved Version of the Pressure Anemometer', *J. Atmos. Oceanic Technol.* **8**, 575–584.

Oost, W. A., Fairall, C. W., Edson, J. B., Smith, S. D., Anderson, R. J., Wills, J. A. B., Katsaros, K. B., and DeCosmo, J.: 1992, 'Flow Distortion Calculations and their Application in HEXMAX', in preparation.

Panofsky, H. A. and Dutton, J. A.: 1984, *Atmospheric Turbulence*, Interscience – J. Wiley & Sons, New York, 397 pp.

Perrie, W. and Toulany, B.: 1990, 'Fetch Relations for Wind-Generated Waves as a Function of Wind-Stress Scaling', *J. Phys. Oceanogr.* **20**, 1666–1681.

Skupniewicz, C. E. and Davidson, K.L.: 1991, 'Hot-Film Measurements from a Small Buoy: Surface Stress Estimates Using the Inertial-Dissipation Method', *J. Atmos. Oceanic Tech.* **8**, 309–322.

Smith, S. D.: 1974, 'A System for Analysis of Time Series Data', Rep. BI-C-74-1, Bedford Inst. of Oceanography, Dartmouth, N.S., Canada, 68 pp.

Smith, S. D.: 1980, 'Wind Stress and Heat Flux over the Ocean in Gale Force Winds', *J. Phys. Oceanogr.* **10**, 709–726.

Smith, S. D.: 1981, 'Factors for Adjustment of Wind Speed over Water to a 10 Metre Height', *Rep. BI-R-81-3*, Bedford Institute of Oceanography, Dartmouth, N.S., Canada, 29 pp.

Smith, S. D.: 1988, 'Coefficients for Sea Surface Wind Stress', *J. Geophys. Res.* **93**, 15467–15472.

Smith, S. D.: 1991, 'Some Early Results of the Humidity Exchange over the Sea Main Experiment', pp. 377–382 in *Deep Convection and Deep Water Formation in the Oceans*, P.-C. Chu and J.-C. Gascard (eds.), Elsevier, Amsterdam.

*Smith, S. D. and Anderson, R. J.: 1988, 'Bedford Institute of Oceanography Eddy Flux Measurements During HEXMAX', in W. A. Oost, S. D. Smith and K. B. Katsaros (eds.), *Proc. NATO Adv. Workshop HEXMAX Analysis and Interpretation*, Dept. of Atmospheric Sciences, University of Washington, Seattle, 243 pp.

Smith, S. D., Katsaros, K. B., Oost, W. A., and Mestayer, P. G.: 1990, 'Two Major Experiments in the Humidity Exchange over the Sea (HEXOS) Program', *Bull. Amer. Meteorol. Soc.* **71**, 161–172.

Snyder, R.L., Dobson, F. W., Elliott, J. A., and Long, R. B.: 1981, 'Array Measurements of Atmospheric Pressure Fluctuations above Surface Gravity Waves', *J. Fluid Mech.* **102**, 1–59.

Stewart, R. W.: 1974, 'The Air-Sea Momentum Exchange', *Boundary-Layer Meteorol.* **6**, 151–167.

Taylor, P. K. *et al.*: 1987, 'RRS Frederick Russell Cruise 9/86, 11 October – 21 November 1986. HEXOS – Humidity Exchange Over the Sea Experiment', Inst. of Oceanographic Sciences, Wormley, U.K., Cruise Report 190, 55 pp.

Wieringa, J.: 1980, 'A Revaluation of the Kansas Mast Influence on Measurements of Stress and Cup Anemometer Overspeeding', *Boundary-Layer Meteorol.* **18**, 411–430.

Toba, Y., Iida, N., Kawamura, H., Ebuchi, N., and Jones, I. S. F.: 1990, 'Wave Dependence of Sea-Surface Wind Stress', *J. Phys. Oceanogr.* **20**, 705–721.

Wills, J. A. B.: 1984, 'HEXOS Model Tests on the Noordwijk Tower', NMI (now: British Maritime Technology Ltd.) Rep. R 184, 56 pp.

Wu, J.: 1980, 'Wind Stress Coefficients over Sea Surface near Neutral Conditions – a Revisit', *J. Phys. Oceanogr.* **10**, 727–740.

Wucknitz, J.: 1980, 'Flow Distortion by Supporting Structures', pp. 605–626 in F. Dobson, L. Hasse and R. Davis (eds.), *Air-Sea Interaction*, Plenum Press, New York and London, 801 pp.

Wyngaard, J. C.: 1981, 'The Effects of Probe-Induced Flow Distortion on Atmospheric Turbulence Measurements', *J. Appl. Meteorol.* **20**, 784–794.

Wyngaard, J. C., Rockwell, L., and Friehe, C. A.: 1985, 'Errors in the Measurement of Turbulence Upstream of an Axisymmetric Body', *J. Atmos. Oceanic Tech.* **2**, 605–614.

Wyngaard, J. C. and Zhang, S.-F.: 1985, 'Transducer-Shadow Effects on Turbulence Spectra Measured by Sonic Anemometers', *J. Atmos. Oceanic Tech.* **2**, 548–558.

Wyngaard, J. C.: 1988, 'The Effects of Probe-Induced Flow Distortion on Atmospheric Turbulence Measurements: Extension to Scalars', *J. Atmos. Sciences* **45**, 3400–3412.

*Available from K. B. Katsaros at University of Washington.